JOURNAL OF THERMOPLASTIC COMPOSITE MATERIALS

Review

Dynamic mechanical analysis of PA 6 under hydrothermal influences and viscoelastic material modeling

Journal of Thermoplastic Composite Materials
2023, Vol. 0(0) 1–35

DOI: 10.1177/08927057231155864
journals.sagepub.com/home/jtc
SAGE

Loredana Kehrer[1], Johannes Keursten[1], Valerian Hirschberg[2] and Thomas Böhlke[1]

Abstract

Polyamides serve as matrix material for fiber reinforced composites and are widely applied in many different engineering applications. In this context, they are exposed to various environmental influences ranging from temperature to humidity. Thus, the influence of these environmental conditions on the mechanical behavior and the associated implications on the performance of the material is of utmost importance. In this work, the thermoviscoelastic behavior of polyamide 6 (PA 6) for two equilibrium moisture contents is investigated. To this end, dynamic mechanical analysis tests with and without humidity control of the environmental chamber were performed. In terms of relaxation tests, the experimental results reveal drying effects and increased diffusion activities when the sample's equilibrium moisture content differs from the ambient humidity level within the testing chamber. Temperature-frequency tests quantify the humidity-induced shift of the glass transition temperature. The linear generalized Maxwell model (GMM) and time-temperature superposition are used to analyze the hydrothermal effects on the linear viscoelastic material properties and the onset of mechanical nonlinearity. Based on these investigations and findings, insight is gained on the humidity influence on the material properties and the limitations of linear thermoviscoelastic modeling. Furthermore, the computational construction of master curves and the parameter identification for a generalized Maxwell model are described in detail.

[1]Institute of Engineering Mechanics, Chair for Continuum Mechanics, Karlsruhe Institute of Technology (KIT), Karlsruhe, Germany
[2]Institute for Chemical Technology and Polymer Chemistry, Karlsruhe Institute of Technology (KIT), Karlsruhe, Germany

Corresponding author:
Loredana Kehrer, Institute of Engineering Mechanics, Chair for Continuum Mechanics, Karlsruhe Institute of Technology (KIT), Kaiserstrasse 10, Karlsruhe 76131, Germany.
Email: loredana.kehrer@kit.edu

Keywords
Time-temperature superposition, viscoelasticity, polyamide 6, humidity influence, DMA, generalized Maxwell model

Introduction

Polymer-based materials are widely used in many engineering fields ranging from the automotive sector to naval applications. As basis for fiber reinforced composites,[1,2] they contribute to high-performance structures while enabling cost-efficient production.[3] There is a large number of polymer matrices in use, which differ greatly in their physical properties. Polyamides in particular have proven their worth as polymeric matrix materials and are increasingly applied due to their outstanding specific mechanical and thermal properties as well as chemical resistances. However, during service, the polymer material may be exposed to harsh environments that limits its use. Due to the hydrophilic nature of the amide functional groups of polyamides, the relative humidity strongly influences the performance of the material which leads to a major challenge in technical applications.[4] In addition to the hygroscopic behavior, the time-, temperature-, and frequency-dependent behavior needs also to be accounted for the viscoelastic material modeling.[5,6]

Viscoelastic material modeling of polyamide 6

Detailed overviews on linear viscoelastic modeling can be found in.[7–9] The basic integral formulation of linear viscoelasticity is given by the Boltzmann superposition integral. Schapery[10] extended this integral expression to model nonlinear viscoelastic behavior of polymers.

In differential formulations, rheological elements are used.[7,9] The basic elements are linear springs and linear dashpots associated with stiffnesses and relaxation (retardation) times, respectively. These elements can be combined to more complex models. The generalized Maxwell model (GMM) and the generalized Kelvin model are often used to model the viscoelastic behavior of polymers.[11] These models are used for strain driven and stress driven processes, respectively. Both models are equivalent and the relations between the models are well known.[11,12] These differential models can be reformulated yielding the Boltzmann superposition integral where the kernel function is given by the so called Prony series. Kießling and Ihlemann[13] used the GMM to model the viscoelastic behavior of PA 6 in the context of large deformations. Koyanagi et al.[14] developed a viscoelastic-viscoplastic material model for PA 6 where a GMM was considered for the viscoelastic part. Under special assumptions, a differential formulation of the nonlinear Schapery model exists.[15,16] In three-dimensional and isotropic formulations of the linear viscoelastic models, a decomposition into spherical and deviatoric parts is used.[12,17,18]

Time-temperature superposition principle

A common approach to model temperature-dependent behavior in the linear viscoelastic regime is to assume thermorheological simplicity.[7,8] For a GMM with multiple elements,

the stiffnesses are independent of temperature whereas relaxation (retardation) times depend on temperature by the same function.[19] In the Boltzmann superposition integral, a reduced time scale is introduced.[7,20]

For isothermal processes, time-temperature superposition (TTS) arises. On a logarithmic scale, viscoelastic properties at various temperatures can be derived by temperature-dependent time (frequency) shifts.[7,19] Experimental measurements at various temperature levels can be combined to master curves with a larger time (frequency) range.[21–23]

The Williams-Landel-Ferry (WLF) equation[24] and the Arrhenius equation are often used to describe the shift function.[25–27] The WLF equation is based on the concept of changes in free volume and is mainly applicable for temperatures above the glass transition temperature θ_g. The Arrhenius equation is often used for temperatures lower than θ_g. Other approaches for shift functions are given by Kristiawan et al.[28] and Shangguan et al.[29]

Thermorheological simplicity can be checked by so called Cole-Cole plots[30] or van Gurp plots.[31–33] In this context, the viscoelastic properties measured by dynamic mechanical analysis (DMA) in temperature-frequency sweeps are used as input. In Cole-Cole plots, the loss modulus is then plotted over the storage modulus. In van Gurp plots, the loss factor is plotted over the dynamic modulus. If thermorheological simplicity is valid, smooth curves result.

If TTS is not applicable, the material behaves thermorheological complex, e.g., in terms of temperature-dependent moduli. This can be modeled by adding a vertical shift.[31,34] A formula for the vertical shift depending on temperature and density can be derived by the Rouse model.[19,35] Brinson and Brinson[7] show that the neglection of vertical shifts can cause large errors in the master curves.

Similar to TTS, other influences like moisture content and load level can also be modeled by shift functions. The influence of water on the material properties of polyamides has been widely studied. In this context, time-moisture content superposition plays an important role.[36–38] Ishisaka and Kawagoe[39] investigated the time-moisture content superposition of PA 6 and epoxy resin based on temperature-frequency tests at different relative humidity levels. In terms of PA 6, the relationship for time-moisture content superposition followed a WLF-type equation. Walter et al.[40] modeled the influence of moisture concentration by a moisture-dependent reference temperature within the WLF equation.

Ferry and Stratton[41] used the concept of changes in the free volume to derive an approach for the dependence of the shift factor on temperature, moisture, and load.[42,43] Many authors use the resulting shift function to apply time-temperature-stress superposition.[44–46] Hadid et al.[47] applied time-stress superposition to multi-step creep tests of PA 6.

Humidity influence on polyamides

In recent years, many different aspects of moisture absorption in PA 6 have been investigated. Among them, for example, the volume and associated geometry change during

water absorption.[48] Since the absorbed water acts as a plasticizer,[49] this leads to a change in the mechanical properties, such as in the glass transition temperature.[50] The amorphous phase of polymers can shift from glassy to rubbery state with water uptake leading to a shift of up towards 60–70 K of the glass transition temperature to lower temperatures.[4] First approaches to predict the glass transition temperature as a function of water uptake were developed by Kelley and Bueche[51] and Reimschuessel.[52]

However, not only the influence of moisture on the thermoviscomechanical properties is of utmost importance but also the inducing mechanisms. In this context, many authors focused on the investigation and modeling of diffusive processes.[53–55] According to Alfrey et al.,[56] diffusion in polymers can be classified by three classes: Fickian (or Case I), non-Fickian (or anomalous), and Case II diffusion. In terms of Fickian diffusion, the rate of diffusion is smaller compared to the rate of relaxation, whereas for Case II the diffusion is much faster than the relaxation. Non-Fickian diffusion is characterized by comparable diffusion and relaxation rates. The mass uptake absorbed at time t can be described by two constants, K and n, reading $M(t) = Kt^n$. In terms of Fickian diffusion, the exponent n reads 1/2. Case II diffusion is characterized by $n = 1$ and non-Fickian diffusion by $1/2 < n < 1$, cf.[56] Nowadays, Case II diffusion is considered as non-Fickian diffusion, such that, generally, one distinguishes between diffusive processes that either obey Fick's law or are described by a non-Fickian diffusion model.

In a semi-crystalline thermoplastic, water plasticizes in amorphous regions between crystalline domains with increased chain mobility.[4,54,57] The Fickian diffusion model (Fick's second law of diffusion) represents the simplest approach to describe the diffusion in or out of the polyamide material. In this context, the temperature dependence of the diffusion coefficient is often described by an Arrhenius equation.[53,54,58] However, for some polyamides, or especially in the glassy state, Fick's law is not applicable.[59] According to the findings of Arhant et al.,[60] the kinetics of the diffusion coefficient in the glassy state (below glass transition temperature) can still be well described by a classical Arrhenius-type equation where the diffusion coefficient depends only on the temperature. In the rubbery state (above glass transition), however, the diffusion coefficient appears to be a function of both temperature and water content which can be captured by the free volume theory.

A detailed overview on the effect of water on polyamides is presented in the review article by Venoor et al.[61]

Sharma et al.[62] developed a finite element model to couple the nonlinear diffusion with viscoelastic material behavior. They simulated the effect of local moisture content on the stiffness of PA 6. A coupling of moisture transport to loading based on a nonlinear diffusion model combined with a linear viscoelastic model is presented in Sharma and Diebels.[63]

Sambale et al.[64,65] investigated the moisture gradient effects on the local material properties based on StepScan DSC measurements and low-energy computer tomography techniques combined with finite element simulations.[66]

Lion and Johlitz[55] presented a thermodynamically consistent approach to model the diffusion of fluids or gases into deformable solids. In this context, the fluid-induced changes in the material properties of the solid are considered. An approach to model the

properties of polymers under hydrothermal conditions close to the glass transition temperature is presented by Engelhard and Lion.[67]

In the context of a nonlinear material model at finite strains, the influence of temperature and moisture content on the viscoelastic material properties of PA 6 was investigated by Kießling and Ihlemann.[13]

Since the influence of water plays an important role when dealing with polyamides, guidelines for sample preparation,[68] conditioning programs,[49,69,70] and experimental treatment were developed.[71]

Motivation and outline

The present work is motivated by the preliminary work on nonlinear viscoelasticity.[16] The overall objective is to develop a nonlinear viscoelastic material model that accounts additionally for hydrothermal influences based on the respective experimental investigations. In this work, however, focus is set on linear viscoelastic modeling and experimental investigations for hydrothermal conditions. The influence of humidity control and no humidity control during a static and dynamic test is discussed. In literature, many experimental investigations of polyamides at different distinct humidity levels are documented. Here, additionally, the influence of humidity during the measurement is observed. Furthermore, implications of the humidity content on the linear-nonlinear transition are addressed. The time-temperature superposition principle is investigated under different humidity levels and correlated with its intrinsic properties, i.e. the glass transition temperature θ_g. Furthermore, some limits of the time-temperature superposition principle are identified. Moreover, a numerical shift algorithm for both vertical and horizontal shifting of the dynamic data to obtain master curves is presented.

The outline of the present work is as follows. First, the mechanical fundamentals as well as the fundamental equations for the thermoviscoelastic characterization by means of dynamic mechanical analysis (DMA) are summarized. The test parameters and sample preparation are presented. Moreover, an enhanced method to automatically evaluate the master curves from temperature-frequency tests based on vertical and horizontal shifting of the data is documented. The experimental results from relaxation, temperature-frequency, and humidity sweep tests are presented and discussed. For the temperature-frequency sweeps, the master curves are determined and presented followed by a discussion on the parameter identification for a generalized Maxwell model by least squares optimization. A summary of the main results and concluding remarks are given in the last section.

Fundamentals

Dynamic mechanical analysis

The thermoviscoelastic material behavior can be characterized by means of dynamic mechanical analysis (DMA). In this context, a distinction is generally made between tests with dynamic and static loads. The tests performed for this work are conducted using the

testing device GABO Eplexor®500N* without humidity control and GABO Eplexor®150N† with the humidity generator Hygromator®. The fundamental equations and principle is shortly summarized in what follows. A detailed overview on DMA is given in Menard.[72]

Static tests

In order to measure the viscoelastic material properties, relaxation tests are performed. Herein, a sample is loaded by a constant strain ε_0 and the material's response is measured resulting in the uniaxial stress-strain response $\sigma(t) = R(t)\varepsilon_0$.[7]

Dynamic tests

A sample is subjected to a cyclic strain or stress load. For dynamic mechanical analysis, this load contains a static preload $\varepsilon_{\text{stat}} = \varepsilon_0$ which is superimposed by a sinusoidal oscillation $\varepsilon_{\text{dyn}} = \Delta\varepsilon \sin(\omega t)$, with $\Delta\varepsilon$ denoting the amplitude, and ω the oscillation frequency of the cyclic load, reading

$$\varepsilon(t) = \varepsilon_{\text{stat}} + \varepsilon_{\text{dyn}} = \varepsilon_0 + \Delta\varepsilon \sin(\omega t) \tag{1}$$

During the test, the amplitude of the sample's deformation as well as the phase shift δ between the cyclic load and the material's response is measured, yielding

$$\sigma(t) = \sigma_0 + \Delta\sigma \sin(\omega t + \delta) \tag{2}$$

Based on the excitation and the material's response, the storage modulus E', representing the instantaneous elastic material response to the oscillation, and the loss modulus E'', representing the viscous behavior induced by internal friction, for instance, can be determined

$$E' = \frac{\Delta\sigma}{\Delta\varepsilon}\cos(\delta), \quad E'' = \frac{\Delta\sigma}{\Delta\varepsilon}\sin(\delta) \tag{3}$$

The ratio of loss and storage modulus yields the loss factor $\tan\delta$. The thermo-viscoelastic material properties can be determined by applying varying temperature and frequency loads to the sample.

Sample preparation

Within this work, two differently conditioned sample states are of interest: dry-as-molded (DAM), and ATM-23/50 conditioned samples. The DAM state is defined by a nominal equilibrium moisture content of less than 0.3wt.%.[73] This state is usually present directly after the manufacturing process and can be maintained by storing samples either in a desiccator or in sealed vacuum bags.[49] In this work, the samples are re-dried in a vacuum oven and stored afterwards in a desiccator.

Additionally, a conditioned state of the samples is of interest for some industrial applications. In this context, conditioning is performed in order to obtain a specific absorption level of water.[74] With respect to polymers, standard atmospheres are defined depending on the application and the polymer considered. The standard atmosphere represents average, non-tropical, laboratory conditions at an equilibrium moisture content between 2.5wt.% and 3.0 wt.%.[6] This state can be accomplished by using a climatic chamber and conditioning programs. In ISO 291,[69] a procedure is described for the standard atmosphere ATM-23/50, i.e. 23°C and 50%RH. However, the ATM-23/50 conditioning procedure is not applicable for PA 6 since, depending on the sample's thickness, the equilibrium moisture content will be achieved after about 1 year (for a 2 mm thickness). In order to overcome this drawback, accelerated conditioning programs have been developed.[70] To meet the technical possibilities of the climatic chamber Memmert ICH110 L used for this work, the conditioning program presented in Jiaet al.[49] is taken into account resulting in an equilibrium moisture content of the samples as obtained by ATM-23/50 conditioning. In this context, the samples of a thickness of 2 mm are stored in the climatic chamber at 55°C and 50%RH (ATM-55/50) for a minimum of 7 days. After this time, the samples are weighed. An equilibrium moisture content is reached if three consecutive weight measurements show a deviation of less than 0.1%.[70] After the equilibrium moisture content is reached, the samples are stored at 23°C and 50%RH (ATM-23/50) until further use.

DMA test parameters

The test parameters for the static tests (relaxation) for ATM-23/50 conditioned samples are listed in Table 1. All samples have the dimensions 83 mm × 10 mm × 2 mm with respect to length, width and thickness. Dynamic tests with varying frequency load and temperature (temperature-frequency tests) are performed for DAM and conditioned (ATM-55/50) samples. The respective testing parameters are given in Table 1 as well.

Linear thermoviscoelastic material modeling

Generalized Maxwell model. In this work, the GMM is used to model linear viscoelastic material behavior. As the experimental characterization is performed by uniaxial tests, a one-dimensional model is considered. The model consists of a linear spring with stiffness E_0 and an arbitrary number N of linear Maxwell elements in parallel. Each Maxwell element consists of a linear spring and a linear dashpot in series. The springs and dashpots are characterized by stiffnesses E_i and viscosities η_i, respectively. In Table 2, the main

Table 1. DMA test parameters for static and dynamic tests. The ratio λ is defined as $\lambda = \Delta\varepsilon/\varepsilon_0$.

Test parameter	Relaxation	Temp.-frequ. test	Humidity sweep
Static load ε_0	0.1%	{0.1%, 0.3%}	0.1%
Ratio λ	–	0.5	0.5
Frequency f	–	0.5 Hz – 50 Hz	5 Hz
Temperature θ	{20, 40, 60, 80}°C	0°C – 200°C	{20, 40, 60, 80}°C
Sample type	ATM-23/50	ATM-23/50, DAM	DAM

equations for the GMM are summarized. The general solution yields the Boltzmann superposition integral.

The analytical solution for a relaxation test with constant strain load is shown in Table 3. The analytical solution for a cyclic strain load is summarized in Table 4. The cyclic stress response is given by the storage modulus and loss modulus that describe the elastic and the viscous behavior, respectively. Their asymptotic characteristics are given by

$$\lim_{\omega \to 0} E' = E_0, \quad \lim_{\omega \to \infty} E' = \sum_{i=0}^{N} E_i, \tag{4}$$

$$\lim_{\omega \to 0} E'' = \lim_{\omega \to \infty} E'' = 0. \tag{5}$$

Time-temperature superposition

Horizontal shift. Often, thermorheological simplicity is assumed to model temperature-dependent viscoelastic behavior. This means that all viscosities of the GMM depend on temperature in the same manner. The stiffnesses are independent of temperature. The viscosities, and consequently the relaxation times, are given by

$$\eta_i(\theta) = a_T(\theta)\eta_i^{\text{ref}}, \ \tau_i(\theta) = a_T(\theta)\tau_i^{\text{ref}}, \ i = 1, \ldots, N \tag{6}$$

Table 2. Summary of the basic equations for the one-dimensional GMM.

Generalized Maxwell model[7,9]	
Spring element	$\sigma_0 = E_0\varepsilon$
Maxwell elements	$\sigma_i = E_i\varepsilon_i^{\text{e}} = E_i\left(\varepsilon - \varepsilon_i^{\text{v}}\right), \ i = 1, \ldots, N$
Viscous strains	$\varepsilon_i^{\text{v}} = \frac{1}{\eta_i}\sigma_i, \ i = 1, \ldots, N$
Evolution equations	$\sigma_i + \frac{1}{\tau_i}\sigma_i = E_i\varepsilon, \ i = 1, \ldots, N$
Partial stresses	$\sigma_i(t) = \int_0^t E_i \exp\left(-\frac{t-s}{\tau_i}\right)\varepsilon(s)\,\mathrm{d}s, \ i = 1, \ldots, N$
General solution	$\sigma(t) = E_0\varepsilon(t) + \int_0^t \sum_{i=1}^{N} E_i \exp\left(-\frac{t-s}{\tau_i}\right)\varepsilon(s)\mathrm{d}s$ $= \int_0^t R(t-s)\varepsilon(s)\mathrm{d}s$

Table 3. Analytical solution for a relaxation test.

Relaxation[7,9]	
Strain load	$\varepsilon(t) = \varepsilon_0$
Stress response	$\sigma(t) = R(t)\varepsilon_0$
Relaxation modulus	$R(t) = E_0 + \sum_{i=1}^{N} E_i \exp(-t/\tau_i)$

Table 4. Analytical solution for a cyclic strain load in a steady state.

Cyclic load[7,9]	
Strain load	$\varepsilon(t) = \Delta\varepsilon \sin(\omega t)$
Strain rate	$\dot{\varepsilon}(t) = \Delta\varepsilon\omega\cos(\omega t)$
Stress response	$\sigma(t) = \Delta\varepsilon\left(E' \sin(\omega t) + E'' \cos(\omega t)\right) = \Delta\varepsilon\lvert E^*\rvert \sin(\omega t + \delta)$
Storage modulus	$E'(\omega) = E_0 + \sum_{i=1}^{N} E_i \frac{(\omega\tau_i)^2}{1+(\omega\tau_i)^2}$
Loss modulus	$E''(\omega) = \sum_{i=1}^{N} E_i \frac{\omega\tau_i}{1+(\omega\tau_i)^2}$
Dynamic modulus	$\lvert E^*\rvert = \sqrt{E'^2 + E''^2}$
Loss factor	$\tan(\delta) = \frac{E''}{E'}$

The temperature-dependent shift function $a_T(\theta)$ has the following properties

$$a_T(\theta_{ref}) = 1,\ a_T(\theta) > 0,\ a_T' < 0. \tag{7}$$

The reference temperature θ_{ref} can be arbitrarely chosen. The temperature-dependent Boltzmann superposition integral reads

$$\sigma(t) = \int_0^t R\big(z(t) - u(s), \theta_{ref}\big)\dot{\varepsilon}(s)\ \mathrm{d}s. \tag{8}$$

In this case, an effective time (reduced time) is defined by[7,20]

$$z(t) = \int_0^t \frac{\mathrm{d}w}{a_T(\theta(w))},\ u(s) = \int_0^s \frac{\mathrm{d}w}{a_T(\theta(w))}. \tag{9}$$

For $\theta > \theta_{ref}$, the material time is faster than the physical time and vice versa. Assuming isothermal processes, $a_T(\theta)$ = const., equation (8) yields

$$R(t,\theta) = E_0 + \sum_{i=1}^{N} E_i \exp\left(-\frac{t}{a_T(\theta)\tau_i}\right) \tag{10}$$

for the relaxation test and

$$E'(\omega,\theta) = E_0 + \sum_{i=1}^{N} E_i \frac{(a_T(\theta)\omega\tau_i)^2}{1 + (a_T(\theta)\omega\tau_i)^2}, \tag{11}$$

$$E''(\omega,\theta) = \sum_{i=1}^{N} E_i \frac{a_T(\theta)\omega\tau_i}{1 + (a_T(\theta)\omega\tau_i)^2}. \tag{12}$$

for the cyclic load case. The expressions t/a_T and ωa_T are called reduced time and reduced frequency, respectively. Then

$$R(t,\theta) = R\left(\frac{t}{a_T},\theta_{ref}\right) = R\left(10^{\log t - \log a_T},\theta_{ref}\right), \tag{13}$$

$$E^{(\cdot)}(\omega,\theta) = E^{(\cdot)}(\omega a_T,\theta_{ref}) \; = E^{(\cdot)}\left(10^{\log\omega+\log a_T},\theta_{ref}\right), \tag{14}$$

with

$$E^{(\cdot)} = E', E'' \tag{15}$$

holds. A deviation from the reference temperature leads to a time (frequency) shift on logarithmic scale. If time or frequency is plotted on the x-axis, a horizontal shift arises. This principle is called time-temperature superposition.

Vertical shift. Thermorheological simplicity can be extended by using an additional vertical shift.[19,34] By introducing $b_T(\theta)$ as vertical shift function, one yields

$$E_i(\theta) = b_T(\theta)E_i^{ref},\; i = 1,\ldots,N. \tag{16}$$

As the shift function is the same for all stiffnesses, equation (10) and (12) are multiplied by this function, reading

$$\tilde{R}\,(t,\theta) = b_T(\theta)R(t,\theta), \tag{17}$$

$$\tilde{E}^{(\cdot)}\,(\omega,\theta) = b_T(\theta)E^{(\cdot)}(\omega,\theta). \tag{18}$$

On a double-logarithmic scale, this leads to an additional vertical shift

$$\log\tilde{R}\,(t,\theta) = \log b_T(\theta) + \log R(t,\theta), \tag{19}$$

$$\log\tilde{E}^{(\cdot)}\,(\omega,\theta) = \log b_T(\theta) + \log E^{(\cdot)}(\omega,\theta). \tag{20}$$

Method of normalized arc length minimization

In experimental testing, a limited range of time (frequency) can be considered. TTS enables to combine experimental data at different temperature levels to obtain a single master curve by shifting. Thereby, viscoelastic behavior can be characterized for a larger time (frequency) range. To avoid manual shifting, numerical shift methods can be applied. The methods found in literature can be grouped in four categories. The method developed by Cho[75] minimizes the arc length of the master curve to determine shift factors.[75–77] The closed form algorithm gives an analytical formula for the shift by setting the area between neighbouring curves to zero.[78–80] The methods of Alwis and Burgoyne,[25] Honerkamp and Weese,[81] and Sihn and Tsai[82] use a combination of polynomial interpolation and

minimization of squared errors. Other methods are based on numerical derivatives of the viscoelastic properties.[83–85] The method used in this work is based on the work by Bae et al.[76] This method is chosen due to its simple implementation and lower requirements to the number of data points. The idea of the method is visualized by Figure 1. In Figure 1(a), two curves are examplarily given. The red curve needs to be shifted and the blue curve serves as reference curve. The shift of the red curve to the final position is shown in Figure 1(b). For an automated method, a quantitative parameter is defined. In this context, the arc length *l(a)* is introduced as a function of the shift a. The method determines the shift that minimizes the arc length. Therefore, global optimization is used

$$l(a) \rightarrow \min_{a \in [a_{\mathrm{L}}, a_{\mathrm{U}}]} . \tag{21}$$

The lower and upper bounds for the shift, a_{L}, a_{U}, are prescribed by the user. Each increment of the global optimization scheme, has the following structure

(i) Define the reference curve by L_1 and the shifted curve by L_2

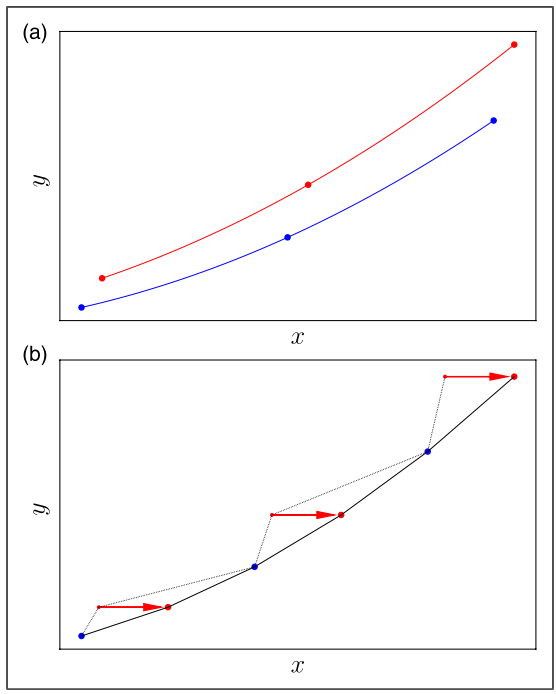

Figure 1. Visualization of the shift method: (a) Initial state of the blue and the red curve. (b) The blue curve serves as reference curve and the red curve is shifted by minimizing the normalized arc length.

$$L_1 = \left\{ \left(x_1^{(1)}, y_1^{(1)}\right), \ldots, \left(x_m^{(1)}, y_m^{(1)}\right) \right\}, \tag{22}$$

$$L_2 = \left\{ \left(x_1^{(2)} + a, y_1^{(2)}\right), \ldots, \left(x_n^{(2)} + a, y_n^{(2)}\right) \right\}. \tag{23}$$

The number of data points in each list is given by m and n, respectively.

(ii) Combine both lists and sort the resulting list by the x-values in ascending order

$$L = L_1 \cup L_2 := \{(x_1, y_1), \ldots, (x_{m+n}, y_{m+n})\}, \; x_1 \leq x_2 \leq \ldots \leq x_{m+n}. \tag{24}$$

(iii) Calculate the normalized arc length

$$l(a) = \sum_{i=1}^{m+n} \sqrt{\left(\frac{x_{i+1} - x_i}{x_{m+n} - x_1}\right)^2 + \left(\frac{y_{i+1} - y_i}{y_{m+n} - y_1}\right)^2}. \tag{25}$$

The method extends the method presented in Bae et al.[76] and Cho[75] by normalizing the partial arc lengths with the total x- and y-range. Thereby, the increasing x-range due to shifting is taking into account, see Figure 1b. By swapping x- and y-data, the method can also be applied for vertical shifts. Dual Annealing optimization, implemented by the `scipy` package in `Python`, is used to solve the minimization problem.

The shift method will be applied to data from temperature-frequency sweeps. The measured $\tan\delta(\omega)$ and $E'(\omega)$ curves at various temperature levels serve as input. First, the horizontal shift factor $a_T(\theta)$ will be determined by using the loss factor since it is not affected by a vertical shift,[35,76,79] cf. Table 4 and equation (18). Starting from the lowest temperature, the relative shifts between neighboring curves are calculated by the shift method with $a \widehat{=} \log a_T^{(\mathrm{rel})}$, $x \widehat{=} \log\omega$ and $y \widehat{=} \tan\delta$. The number of temperature levels is denoted by n_θ. The results are given by

$$\log a_T^{(\mathrm{rel})}(\theta_i), \; \theta_i < \theta_{i+1}, \; i = 2, \ldots, n_\theta. \tag{26}$$

The relative shift at the lowest temperature is set to zero. The total shifts are then calculated by

$$\log a_T(\theta_i) = -\log a_T^{(\mathrm{rel})}(\theta_{\mathrm{ref}}) + \sum_{j=1}^{i} \log a_T^{(\mathrm{rel})}(\theta_j), \tag{27}$$

for $i = 1, \ldots, n_\theta$. The reference temperature can be arbitrarely chosen from θ_i. In a second step, the vertical shift is determined. In this context, the above described procedure is repeated with $a \widehat{=} \log b_T^{(\mathrm{ref})}$, $x \widehat{=} \log E'$ and $y \widehat{=} \log\omega$.

Parameter identification

The last step is to identify parameters for a GMM based on given master curves. This means that a set of $2N + 1$ parameters must be identified

$$\tilde{\mathcal{P}}_N = \{E_0, E_1, \ldots, E_N, \tau_1, \ldots, \tau_N\}. \tag{28}$$

In general, this is an ill-posed problem as no unique solution exists.[32,86,87] This problem can be solved by prescribing a distribution of relaxation times.[88] Jalocha et al.[88] developed a method that finds an optimal distribution of relaxation times. In this work, a logarithmic distribution is used.[89,90] Then, only $N + 1$ stiffnesses need to be identified

$$\mathcal{P}_N = \{E_0, E_1, \ldots, E_N\}. \tag{29}$$

The number N of Maxwell elements is also prescribed. As a rule of thumb, at least one element per considered frequency decade should be used.[87,91] Least squares minimization is used to solve the problem.[88,89,91] Previously, four viscoelastic properties (E', E'', $|E^*|$, $\tan\delta$) were introduced for the dynamic load case. Only two of these properties are independent. Here, storage and loss modulus are used as input for the residual.[88,89,91] Formally, the master curves are defined by the data points $\{\omega_i, E_i'\}$ and $\{\omega_i, E_i''\}$, $i = 1, \ldots, n_\omega$, where n_ω represents the number of data points. The residual is given by

$$r^2(\mathcal{P}_N) = a' \sum_{i=1}^{n_\omega} \left(\frac{E_i' - E'(\omega_i, \mathcal{P}_N)}{E_i'} \right)^2 + a'' \sum_{i=1}^{n_\omega} \left(\frac{E_i'' - E''(\omega_i, \mathcal{P}_N)}{E_i''} \right)^2. \tag{30}$$

The coefficients a' and a'' allow to weight the residuals of storage and loss modulus.[92] The constraints

$$a' + a'' = 1, \; a' > 0, \; a'' > 0 \tag{31}$$

are considered. The `scipy` package in `Python` is used to determine an optimal stiffness distribution by a gradient-based optimization method (L-BFGS-B). The stiffnesses are forced to be non-negative. The quality of the identification is evaluated by the coefficient of determination (R^2-value)

$$R^2 = 1 - \frac{\sum_{i=1}^{n_\omega} \left(E_i^{(\cdot)} - E^{(\cdot)}\left(\omega_i, \mathcal{P}_N^{\text{fit}}\right) \right)^2}{\sum_{i=1}^{n_\omega} \left(E_i^{(\cdot)} - \overline{E}^{(\cdot)} \right)^2}, \tag{32}$$

$$\overline{E}^{(\cdot)} = \frac{1}{n_\omega} \sum_{i=1}^{n_\omega} E^{(\cdot)}. \tag{33}$$

Usually, $0 \leq R^2 \leq 1$ holds. The larger the value of R^2, the better the fit.[93]

Experimental investigations

In this section, results are presented focusing on dynamic and static loads and the influence of humidity load on the mechanical properties. Since the material parameters are sensitive to the sample's moisture content and, thus, the sample's thickness,[64] the respective thickness of the sample used for the experiments is documented in the Appendix. Temperature-frequency tests are performed for ATM-23/50 conditioned PA 6. The experimental data exhibit quantitative evaluation of the viscoelastic properties that serve in what follows as input for the GMM. Relaxation tests indicate not only the viscoelastic behavior but also how diffusive processes during measurement influence the material's response. Moreover, humidity sweep tests are chosen to show the influence of hydrothermal loads on the mechanical properties.

Relaxation tests

Considering ATM-23/50 conditioned samples, relaxation tests at different temperatures are performed. The test parameters are given in Table 1. The tests for $\theta = \{20, 40, 60, 80\}$° C are performed with the testing device GABO Eplexor®500N without humidity control. Thus, the equilibrium moisture content of a sample might, in general, differ from the ambient humidity content within the testing chamber. Additionally, a test at $\theta = 80$°C is repeated with the testing device GABO Eplexor®150N with the humidity generator Hygromator®. In this context, the ambient humidity level is set to equal the ATM-23/50 sample's moisture content of $\Phi = 50$%RH. By this, the difference between humidity control versus no humidity control, i.e. the impact of diffusion, with respect to relaxation tests can be illustrated. In order to exclude influences of the thermal expansion of the crosshead during the measurement, each sample was held at the target temperature for 1 h prior to the relaxation test. After this so-called soak time, the relaxation test was performed. The measurement time presented in this work ranges up to 6 h.

In Figure 2, the experimental results of the relaxation modulus $R(t)$ are depicted. Considering first the data from the tests without humidity control, for all four temperature loads and up to a measurement time of nearly 500 s, $R(t)$, and, thus, $\sigma(t)$, decreases in a typical manner. However, for $t \geq 500$ s and higher temperatures, $R(t)$ increases again after the initial decrease. As the environmental chamber of the DMA testing device exhibits an ambient humidity content of approximately 35%RH, drying of the sample takes place during the test. The chain mobility of polyamides is affected not only by humidity but also by temperature, i.e., the diffusion velocity increases with increasing temperatures.[61] Consequently, the diffusion and drying effects are more pronounced for samples at a higher temperature and are detected by an increase of the $R(t)$ curve. Directly before and after the relaxation tests, each sample is weighted. The change in weight is documented in Table 5. For the sample tested at 20°C no significant change in weight is observed, whereas with increasing testing temperature, the samples looses up to 1.115% of weight at 80°C by drying during the measurement. In contrast, considering the experimental results for the test with humidity control ensured by the humidity generator, the relaxation modulus decreases for the total considered time range in a typical manner. Up to 400 s, the

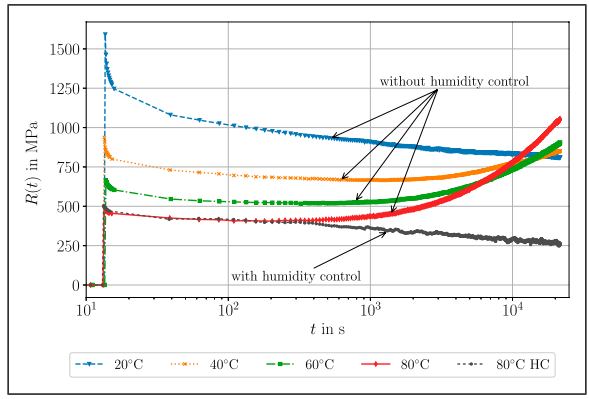

Figure 2. Relaxation modulus depicted over logarithmic time obtained from relaxation tests with ATM-23/50 samples with and without humidity control. HC: humidity control.

Table 5. Weight of the samples from the relaxation tests at different temperatures before and after the DMA measurement. The relative deviation Δm is determined by $\Delta m = (M_{end} - M_{initial})/M_{initial}$.

Humidity control	Temperature, °C	$M_{initial}$, g	M_{end}, g	Relative deviation Δm
no	20	1.9452	1.9451	−0.0051%
no	40	1.9484	1.9431	−0.272%
no	60	1.9469	1.9349	−0.616%
no	80	1.9467	1.9250	−1.115%
yes	80	1.9534	1.9532	−0.0102%

curves for $\theta = 80°C$ with and without humidity control nearly coincide. However, as the measurement time increases, the curves diverge, highlighting the effects of sample drying and increasing diffusion activities. In many publications, relaxation (or creep) tests are performed for a duration of far less than 400 s. Water sorption during this time does not appear to significantly affect the material behavior, however, for longer periods in the range of hours, a humidity-controlled environmental chamber is meaningful.

Temperature-frequency tests

For a DAM sample, temperature-frequency tests with test parameters according to Table 1 are performed. The results for the storage modulus E' and the loss factor $\tan\delta$ over temperature are depicted in Figure 3. The storage modulus shows a highly temperature-dependent behavior, see Figure 3(a), by decreasing strongly with increasing temperature. The decrease from the maximal value of E' at 0°C to the minimal value at 200°C is about 90%. Within the range $50°C \leq \theta \leq 100°C$, a pronounced dependency on the applied frequency load is shown indicating increasing viscoelastic effects. Generally, E' exhibits

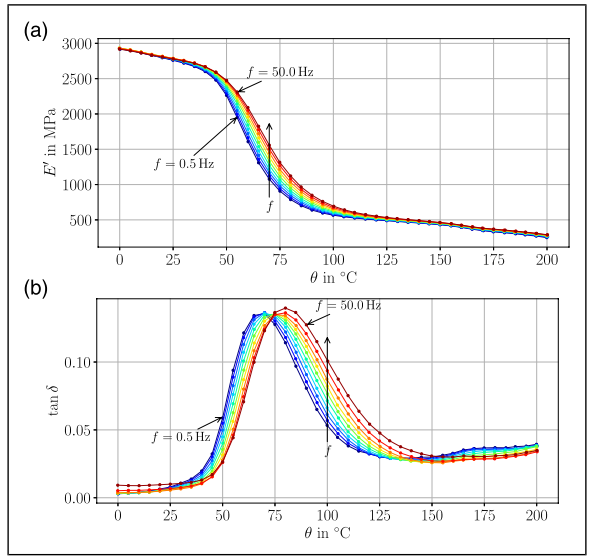

Figure 3. Temperature frequency tests with DAM sample for 0°C ≤ θ ≤ 200°C and 0.5 Hz ≤ f ≤ 50 Hz. (a) Storage modulus E' over temperature load revealing thermoviscoelastic material behavior. (b) Loss factor $\tan\delta$ over temperature indicating frequency-dependent glass transition temperature.

higher values for higher frequency loads throughout the temperature range considered. In Figure 3(b), the loss factor $\tan\delta$ is depicted over the temperature exhibiting the characteristic shape for polymer-based materials: First, a nonlinear increase of the $\tan\delta$ curve is shown for increasing temperatures until a peak is reached. After the peak, the curve is decreasing again. There are at least five common methods to determine θ_g as stated in Ehrenstein.[94] In this work, the maximum in the loss factor curve is considered to mark the glass transition temperature θ_g. The loss factor exhibits a frequency-dependent behavior, analogously to E'. Considering the lowest and highest frequency load of 0.5 Hz and 50 Hz, respectively, the glass transition temperature θ_g is shifted by 10 K from nearly 70°C to 80°C.

The temperature-frequency test was repeated using a ATM-23/50 conditioned sample. In Figure 4, the experimental data for both ATM-23/50 and DAM samples are depicted for E' and $\tan\delta$ considering a frequency load of 5 Hz. The data of the ATM-23/50 samples are shifted towards lower temperatures when compared to the DAM data. The glass transition temperature θ_g is shifted by about -50 K from approximately 75°C (DAM) to 25°C (ATM-23/50). Moreover, the values for $\tan\delta$ at θ_g are smaller for ATM-23/50 data than for DAM data. The comparison reveals the effect of humidity on the glass transition as reported in literature.[61]

The difference in moisture between a sample and its environment leads to an inhomogeneous moisture content throughout the sample's thickness and, thus, induces locally

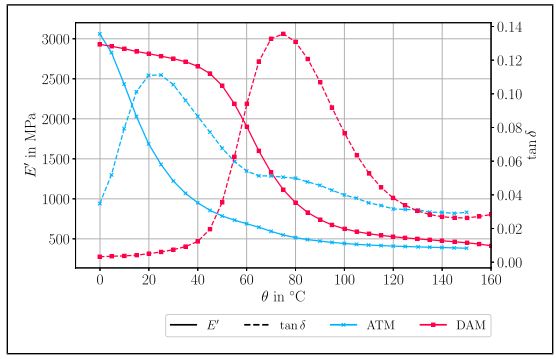

Figure 4. Comparison of storage modulus E' and loss factor $\tan\delta$ over temperature for $f = 5$ Hz and samples with two different moisture contents (ATM-23/50 and DAM). The higher equilibrium moisture content in the sample shifts the curves and glass transition to lower temperatures.

varying material properties. A significant moisture gradient throughout the sample's thickness is reported in Figure 17 of Sharma et al.[62] Their simulations reveal that a homogeneous distribution of the moisture content within the sample is reached only after several hours or days, depending on the considered moisture boundary conditions. In Figure 18 of Sharma et al.,[62] an essential influence of the moisture distribution on the mechanical properties is reported. However, despite the impact of the moisture distribution on the material behavior, they also showed that for loadings in the range of small deformations, $\varepsilon < 0.5\%$, the heterogeneous moisture distribution has a less significant effect on the overall structural properties, i.e. the effective properties, of the specimen. With respect to the present work, it should be noted that in all tests where ambient humidity is not controlled, a moisture gradient is to be expected within the sample. However, it is assumed that this gradient, especially within the loading regime considered here for the relaxation and temperature-frequency tests, will not significantly affect the measured effective material properties at sample scale. Thus, the experimental results within this work are to be understood as effective properties. Locally distributed material properties due to the possible inhomogeneous moisture distribution are not considered, here.

Humidity sweep

For the investigation of the humidity influence on PA 6, DAM samples are subjected to a dynamic load. Within the environmental chamber, the ambient humidity level varies between 5%RH and 95%RH with a rate of 1%RH/min at a controlled temperature. For temperatures at 20°C, 40°C, 60°C, and 80°C, the storage modulus over the ambient relative humidity content Φ within the environmental chamber is depicted in Figure 5. As illustrated by the graphs in Figure 5, the storage modulus decreases with increasing humidity level. Note that the experimental data obtained from this experiments are not

at an equilibrium moisture state but are rather continuously changing. Moreover, due to the continuous change in the humidity level, a gradient of the moisture level within the sample is expected. However, within this work, the data are regarded as effective properties and local inhomogeneities are not taken into account. The effect of gradient moisture distribution on local mechanical properties is discussed in detail by Sambale et al.,[64,65] and on viscoelastic properties by Sharma et al.[62]

Table 6 lists the quantitative difference between the values of E' at the beginning and at the end of the measurements for the four different temperatures. At room temperature, the influence of the relative surrounding humidity on the sample appears to be not as significant since here diffusion processes are not within the time scale of the measurement. However, with increasing temperatures, the relative deviation between the initial and final value of E' increases indicating a strong influence of the humidity on the mechanical behavior at temperatures around θ_g. Since for 80°C the humidity level of 95%RH could not be reached, the relative deviation is in this case smaller than for 60°C but is expected to be in the same range. When comparing the difference in E' for humidity load and thermal

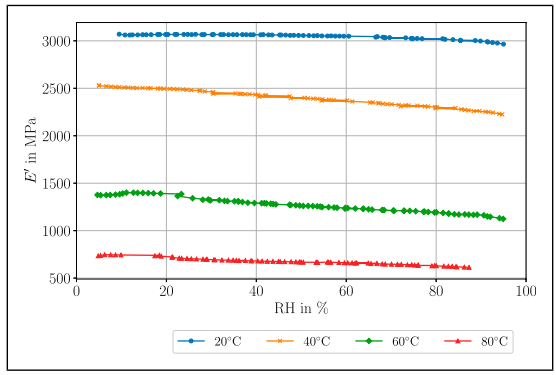

Figure 5. Storage modulus E' over ambient relative humidity content in the environmental chamber at four different temperature loads shows influence of the hydrothermal load on the material's response. Humidity tests are performed with GABO Eplexor®150N with the humidity generator Hygromator®.

Table 6. Values of the storage modulus E' at the beginning and end of the humidity sweep measurement. The relative deviation ϵ is determined by $\epsilon = (E'(\Phi_{end}) - E'(\Phi_{initial}))/E'(\Phi_{initial})$.

θ, °C	$E'(\Phi_{initial})$, MPa	$E'(\Phi_{end})$, MPa	Rel. deviation ϵ
20	3070.23	2965.34	−3.42%
40	2533.25	2230.29	−11.96%
60	1376.23	1123.94	−18.33%
80	734.776	612.969	−16.58%

load, the influence of temperature appears as more significant since the drop in E' is about 76% considering exemplarily $\Phi = 20\%$RH and the experimental data for 20°C and 80°C.

Simulation results

Master curve construction

The validity of TTS is checked by Cole-Cole plots and shown for DAM samples in the Appendix. The next step is to construct the master curves by the method described previously. Figures 6 and 7 exemplarily show the shift procedure for a temperature-frequency sweep. The reference temperature is set to $\theta_g = 75$°C. In Figure 6, the horizontal shifting (step I) is

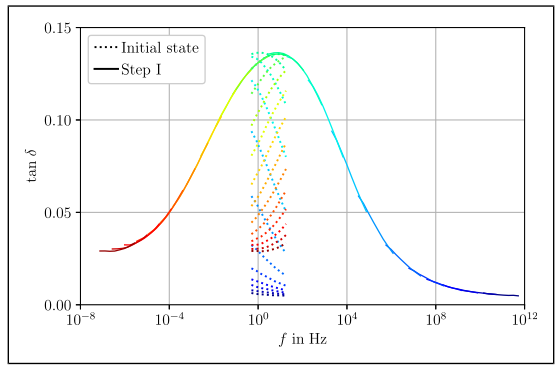

Figure 6. Horizontal shifting is applied to loss factor data. The dotted lines show the unshifted data at various temperatures. The solid lines represent the horizontally shifted data. From the blue to the red lines, temperature is increasing. The reference temperature is 75°C.

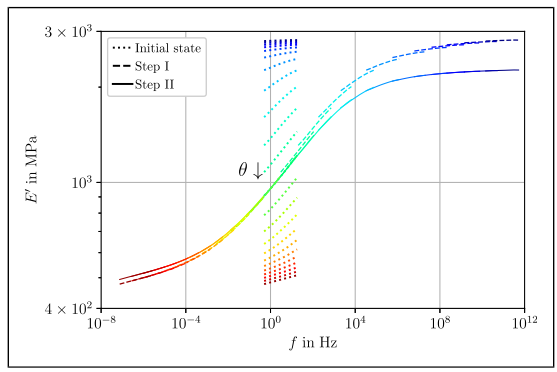

Figure 7. Horizontal and vertical shifting is applied to storage modulus data. The dotted lines show the input data. The dashed lines result after horizontal shifting. Adding vertical shifts leads to the solid lines. The reference temperature is 75°C.

illustrated. In the initial state, the individual curves for various temperature levels can be seen. These curves are shifted horizontally. Then, the plot of the loss factor shows a smooth master curve. At reference temperature, both curves coincide. The highest temperature level (130°C) is at the left end, the lowest level (20°C) at the right end. In Figure 7, it can be seen that after step I the plot of the storage modulus is still not smooth. Thus, vertical shifting (step II) is necessary and results in a smooth master curve. The loss factor is not influenced by step II. In Table 7, the considered frequency and temperature ranges for each test are shown. Additionally, the corresponding reference temperature is listed. In all cases, the highest frequency levels are neglected to obtain smooth master curves. Thus, TTS is limited to a physical frequency lower than 20 Hz. This does not contradict the plots in Figures 6 and 7 since these plots include frequencies above the limit of 20 Hz in the sense of reduced frequencies. With increasing moisture, the temperature range, in which TTS is applicable, is shifted to lower temperatures. This can be seen by comparing DAM and ATM samples. For $\varepsilon_0 \leq 0.3\%$, TTS is valid and the limitations in temperature and frequency range are not affected by the load level.

Comparison of different master curves

In Figures 8 and 9, master curves obtained from dynamic tests are shown. Storage modulus and loss modulus are plotted on a double-logarithmic scale. The reference temperature is set to the corresponding approximated glass transition temperature for each curve, $\theta_{ref} = 75°C$ for DAM samples without humidity control, $\theta_{ref} = 60°C$ for DAM samples with humidity control, and $\theta_{ref} = 25°C$ for ATM samples.

Figure 8 depicts the master curves of the tests performed without humidity control. In terms of a linear viscoelastic behavior, the curves should be identical for different load levels. As the red and the blue curves are not identical, the dried samples show nonlinear behavior at a mean strain $\varepsilon_0 = 0.3\%$. A load shift cannot be applied as the curve shapes differ. On the red curve, the saddle point of the storage modulus and the maximum of the loss modulus is reached for a higher frequency. Furthermore, the loss modulus is not symmetric as it decreases less strongly after its maximum is reached. Additionally, the shift factors for the higher load are larger resulting in a broader frequency range. For the conditioned samples, nonlinear behavior cannot be detected as the master curves are in good agreement.

Table 7. Master curve construction: Considered temperature and frequency ranges.

Conditioning	Static load ε_0	Frequency f, Hz	Temperature θ, °C	θ_{ref}, °C
DAM	0.1%	0.5 – 18	20 – 130	75
DAM	0.3%	0.5 – 18	20 – 130	75
DAM	0.5%	TTS invalid		
ATM	0.1%	0.5 – 10.8	0 – 95	25
ATM	0.3%	0.5 – 10.8	0 – 95	25
DAM, Φ = 20%RH	0.1%	0.5 – 19.9	10 – 70	60
ATM, Φ = 50%RH	0.1%	0.5 – 19.9	10 – 70	25

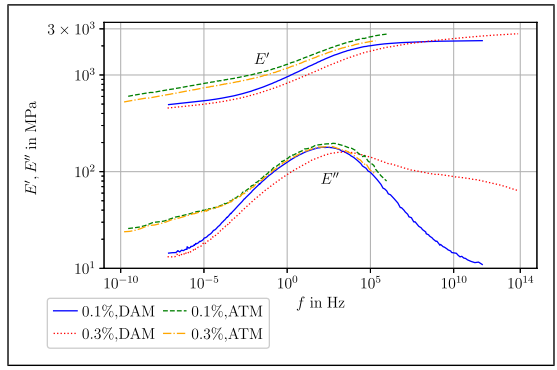

Figure 8. Master curves for ATM-23/50 (θ_{ref} = 25°C) and DAM samples (θ_{ref} = 75°C) obtained from temperature-frequency tests at mean strains of 0.1% and 0.3% without humidity control.

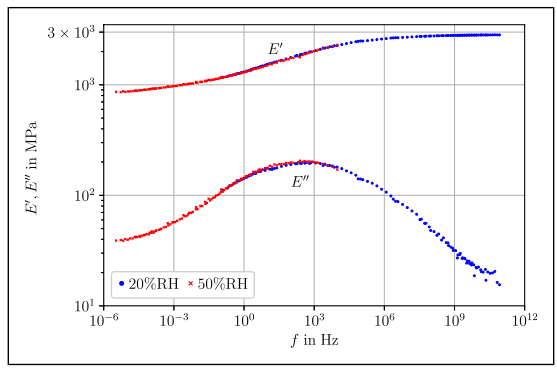

Figure 9. Master curves obtained from temperature-frequency tests at mean strains of 0.1% with humidity control. Tests were performed with an ATM-23/50 conditioned sample at 50%RH (θ_{ref} = 25°C) and with a DAM sample at 20%RH (θ_{ref} = 60°C).

The master curves shown in Figure 9 provide a common master curve. In this case, the humidity influence can be modeled by a humidity-dependent glass transition temperature. If instead the same reference temperature is chosen for both master curves, a humidity shift can be seen. The master curves for the tests without humidity control in Figure 8 indicate more complex nonlinear behavior. Only the loss modulus shows a common master curve between 10^{-1} Hz and 10^6 Hz. Therefore, the influence of moisture content cannot be modeled by a simple shift in this case.

In Figure 10, the master curves for tests of ATM23/50 conditioned samples with and without humidity control are compared. The curves are in good agreement. In this case, the influence of a missing climate control is not as pronounced. Consequently, changes in mechanical properties due to diffusion do not happen at the measurement temperatures ($10 - 70$°C) within the time scale of the experiment. This is in agreement with Figure 2

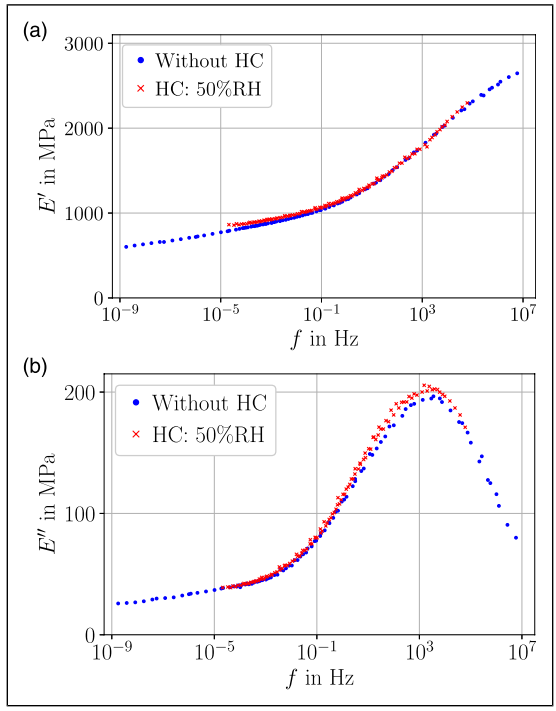

Figure 10. Comparison of master curves from tests performed with humidity control (HC) at 50%RH and without humidity control. ATM-23/50 conditioned samples were used, θ_{ref} = 25°C. (a) Storage modulus. (b) Loss modulus.

where, for instance, at 80°C no differences were observable for the first 400s of the relaxation test. Note, the sample is subjected to the target temperature for about 4000 s in total if the soak time before the starting of the relaxation test is taken into account.

In general, the curves agree well with the asymptotic properties given by equation (5). With increasing moisture content, not all of these properties are evident. The reason is that the corresponding master curves are cut off at some point as the considered temperature range is limited. In all curves, the loss modulus has a pronounced maximum at medium frequencies.

Parameter identification

The discussed master curves can be used as input for a parameter identification. The parameter identification is exemplarily discussed for the tests with DAM samples since these tests cover all properties from equation (5). The relaxation times are prescribed in a logarithmic distribution. First, the load case with $\varepsilon_0 = 0.1\%$ is considered. The largest relaxation time is set to the inverse of the minimum frequency decade, $\tau_N = 10^7$ s. Vice versa, the smallest relaxation time, τ_1, is set to 10^{-12} s. For the stiffnesses, lower and upper

bounds are defined: The lower bound is set to zero as negative stiffnesses are unphysical. The upper bound is set to 2500 MPa which is nearly the maximum storage modulus. The start values for the optimization are also set to zero. The influence of the number of Maxwell elements and of the weighting factors is investigated. In Figure 11, results are shown for various parameters. The black points depict the master curves. The curves in blue and red show the behavior predicted by the parameter fit. Additionally, the R^2-values from equation (33) are given. By increasing the number of Maxwell elements, the fit becomes more precise and smooth, see Figure 11(a), 11(c) and 11(e). Each Maxwell element causes a saddle point in the storage modulus and a local maximum in the loss modulus. The respective positions are defined by the inverse of the corresponding relaxation time. If the number of relaxation times increases, these local saddle points and

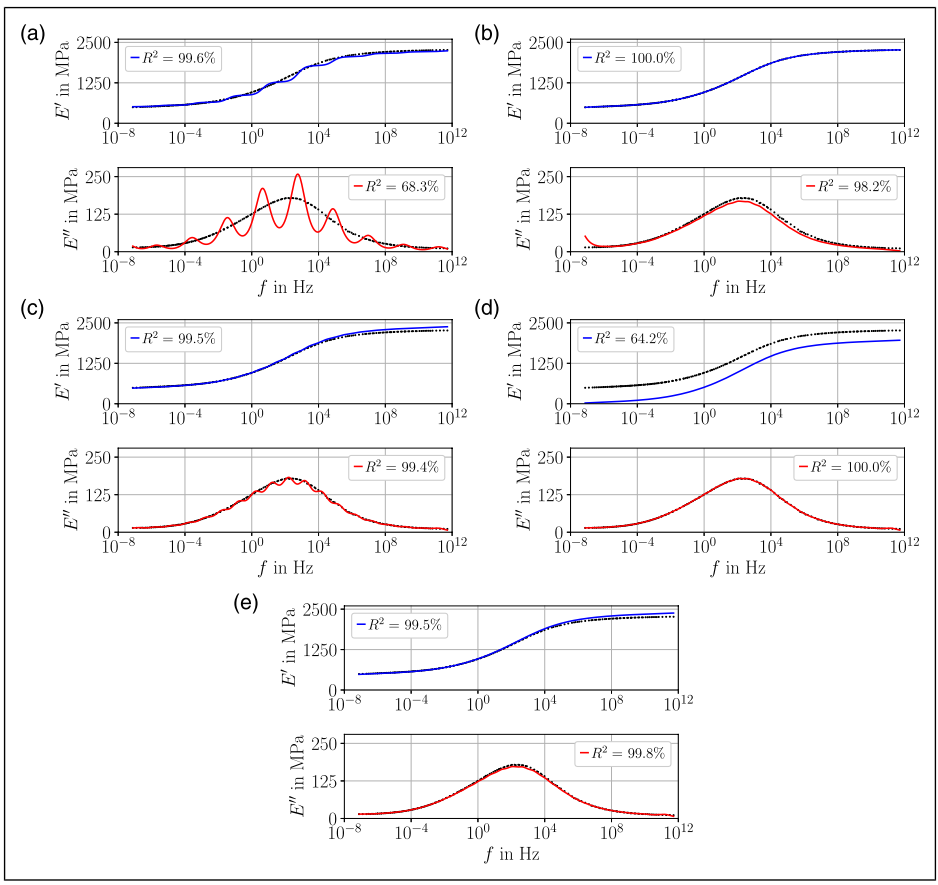

Figure 11. Parameter fit for DAM sample at $\varepsilon_0 = 0.1\%$, $\theta_{\text{ref}} = 75°\text{C}$. Various weighting factors and number of Maxwell elements are considered. The R^2-value is given to quantify the quality of the fits. (a) 10 Maxwell elements, $a' = 50\%$, (b) 30 Maxwell elements, $a' = 100\%$, (c) 20 Maxwell elements, $a' = 50\%$, (d) 30 Maxwell elements, $a' = 0\%$, (e) 30 Maxwell elements, $a' = 50\%$.

maxima are blurred. By using 20 elements, a good fit is already obtained. Thus, the rule of thumb that at least one Maxwell element per frequency decade should be used is confirmed.[87,91] If 30 Maxwell elements are used, only the global saddle point and the global maximum can be seen. For large frequencies, the storage modulus is slightly overestimated. The maximum of the loss modulus is slightly underestimated.

In Figure 11(b), only the storage modulus is considered for the parameter identification, $a'' = 0$. Consequently, E' is perfectly fitted. However, E'' is poorly fitted for low frequencies and slightly underestimated in the frequency range of 10^{-1} to 10^{12} Hz. In contrast, the results for choosing only the loss modulus as input of the parameter identification, $a' = 0$, are depicted in Figure 11(d). In this case, the loss modulus is perfectly fitted. For the storage modulus, an offset can be seen. The reason is indicated by the formula for the loss modulus in Table 4. The loss modulus does not depend on the stiffness of the single spring element E_0. Thus, the start value of E_0 does not change during the optimization. The offset can be minimized by choosing an appropriate start value. To conclude, both storage and loss modulus should be used as input parameters for the parameter identification. Using $a' = a'' = 0.5$ is a reasonable approach.

Figure 12 shows the corresponding stiffnesses and relaxation times for the parameter fits of Figure 11(a), 11(c) and 11(e). The solid lines visualize the respective values of E_0. As E_0 is the lower bound of the storage modulus, the value of E_0 does not change significantly by increasing the number of Maxwell elements. The stiffnesses of the Maxwell elements decrease by increasing the number of Maxwell elements. The maximum of these stiffnesses coincides with the saddle point of E' and the maximum of E'' at medium relaxation times.

In Figure 13, a parameter fit for $\varepsilon_0 = 0.3\%$ is shown. Compared to Figure 11(e), the storage modulus is more overestimated at high frequencies. The reason may be the asymmetric behavior of the loss modulus. To capture this, the stiffnesses at the corresponding relaxation times are larger. This leads to an overestimation of the storage modulus. Espacially for larger frequencies, the GMM cannot capture this behavior

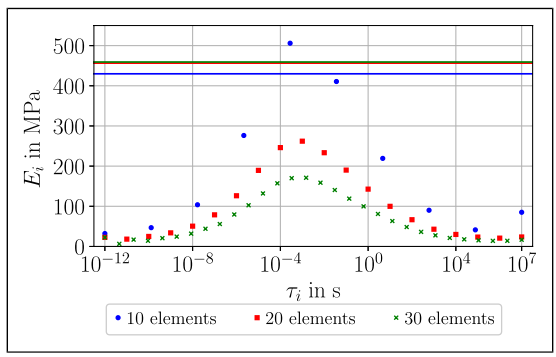

Figure 12. Plot of Maxwell parameters from Figure 11 for $a' = a'' = 0.5$ and various numbers of Maxwell elements: $N = 10$ (blue), $N = 20$ (red), $N = 30$ (green). The solid lines show the value of E_0. The dots show the relaxation times and the corresponding stiffnesses of the Maxwell elements.

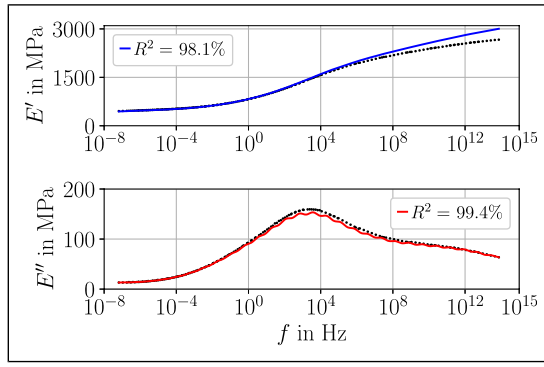

Figure 13. Parameter fit for DAM sample at $\varepsilon_0 = 0.3\%$, $\theta_{ref} = 75°C$. 30 Maxwell elements are used and the residuals are weighted equally: $a' = a'' = 0.5$.

accurately. The corresponding values of the stiffnesses and relaxation times for Figures 11(e) and 13 are given in Table 8 and Table 9.

Summary and conclusion

Polyamide 6 is widely applied as polymeric matrix for fiber reinforced polymers to contribute to a resource-efficient semi-structural material. Despite the outstanding properties of low weight and high specific stiffness accompanied by design freedom for structural parts, PA 6 exhibits also some challenges when environmental influences are taken into consideration. Based on the internal, equilibrium moisture content within the sample, for instance, the characteristic material properties, such as the glass transition temperature, are shifted. In order to take these and other effects into account, the material model needs to be adapted accordingly. Within this work, the thermoviscoelastic material properties for two different humidity levels of PA 6 are experimentally investigated using DMA. By means of the generalized Maxwell model, the hydrothermal effects on the linear viscoelastic material behavior are analyzed. To this end, the following concluding remarks can be made.

Experimental investigations

Relaxation tests. In this context, the tests were performed with and without humidity control inside the testing chamber for a duration of 6 h. For the humidity-controlled tests, the ambient and the internal equilibrium moisture of the sample were the same. In case of no humidity control, after an initial decrease of the relaxation modulus, an increase was observed after 500 s. As per conditioning, the samples exhibited an initial relative humidity of 50%RH, whereas the relative humidity in the testing device chamber was at 35%RH due to environmental conditions. This difference in relative humidity caused a drying of the sample during the measurement inducing changes in the mechanical

properties due to the hydrophilic nature of PA 6. A direct comparison between the experiment conducted at controlled and non-controlled humidity, further illustrated this effect. While in the humidity-controlled test no drying of the sample takes place, a typical decreasing course over time results for the relaxation modulus. Consequently, for relaxation tests at times within the range of hours, use of a humidity-controlled testing chamber is recommended.

Temperature-frequency tests. To determine the viscoelastic behavior of the PA 6 material used within this work and to obtain input data for a viscoelastic material model based on generalized Maxwell elements, DMA tests with varying temperature and frequency load were conducted. The evaluation of these tests revealed that the glass transition temperature is shifted by about 10 K for a considered frequency range of three decades. However, a higher influence on the glass transition temperature by humidity load was observed. A comparison between DAM and ATM-23/50 conditioned samples revealed a shift of 50 K for the glass transition temperature.

Humidity sweeps. DMA tests with varying ambient humidity level ranging from 5%RH to 95%RH were performed. The tests were repeated at four different temperatures. The temperature load showed a more significant influence on the storage modulus E' than the humidity load, however, it should be noted that the samples did not reached equilibrium moisture content during the measurements.

Viscoelastic modeling and parameter identification

Shift method. Based on the method by Bae et al.,[76] the method of normalized arc length minimization was developed. To account for an increasing x-range by the shifting procedure, the existing method was extended by using the normalized arc length. The method calculates shift factors by global optimization and was applied to temperature-frequency tests. First, horizontal shift factors were determined based on the loss factor. Then, vertical shift factors were calculated based on the storage modulus.

Master curves. Master curves were constructed for various loading conditions and then compared. The following limitations of TTS could be observed:

- TTS failed for DAM sample at a mean strain of 0.5% and an amplitude of 0.25%
- The temperature range for DAM samples was between 20°C and 130°C
- This temperature range is shifted by approximately −30 K for conditioned samples
- Frequencies higher than 20 Hz were not considered

For DAM samples, a load-dependency of the master curves was observed. For the conditioned samples, no pronounced load dependence was detected. By comparing the test performed under humidity control at 50%RH and the test with a conditioned sample, no differences were evident. In contrast to the findings based on the relaxation tests with and without humidity control, a humidity-controlled testing chamber is not necessarily required

for temperature-frequency tests. The testing time is within time scales where diffusive processes are not that pronounced as to cause significant differences between test data.

Parameter identification. The master curves of the DAM samples were exemplarily used as input for a GMM parameter identification. The weighted residuals of storage modulus and the loss modulus were considered for least squares optimization. It was shown that both, storage and loss modulus, should be accounted for. Furthermore, it was confirmed that between one and two Maxwell elements per frequency decade are needed for a good fit. For a mean strain of 0.1%, a good fit is observed. At a mean strain of 0.3%, the fit revealed inaccuracies. This implicates a transition to the nonlinear viscoelastic regime which is the scope of future work.

Acknowledgements

The research documented in this manuscript has been funded by the Deutsche Forschungsgemeinschaft (DFG, German Research Foundation), project number 255730231, within the International Research Training Group "Integrated engineering of continuous-discontinuous long fiber reinforced polymer structures" (GRK 2078/2). The support by the German Research Foundation (DFG) is gratefully acknowledged. Special thanks go to Johanna Heyner for performing the temperature-frequency test for the DAM sample, depicted in Figure 3.

Author contributions

Loredana Kehrer: Conceptualization; project administration; investigation; experiments; formal analysis; visualization; writing - original draft
Johannes Keursten: Conceptualization; parameter identification; methodology; simulation; visualization; writing - original draft
Valerian Hirschberg: Conceptualization; resources; writing - original draft
Thomas Böhlke: Supervision; funding acquisition; writing - editing and review

Declaration of conflicting interests

The author(s) declared no potential conflicts of interest with respect to the research, authorship, and/or publication of this article.

Funding

The author(s) disclosed receipt of the following financial support for the research, authorship, and/or publication of this article: This work was supported by the Deutsche Forschungsgemeinschaft (DFG-GRK 2078/2, project number 255730231).

Notes

* Measurements were performed at the laboratory of the Institute of Engineering Mechanics, Chair for Continuum Mechanics at Karlsruhe Institute of Technology (KIT).
† Measurements were performed at the laboratory of the Institute for Chemical Technology and Polymer Chemistry, Karlsruhe Institute of Technology (KIT).

ORCID iD

Loredana Kehrer https://orcid.org/0000-0002-5712-6515

References

1. Kehrer L, Wood JT and Böhlke T. Mean-field homogenization of thermoelastic material properties of a long fiber-reinforced thermoset and experimental investigation. *J. Compos. Mater* 2020; 54(25): 3777–3799.
2. Trauth A, Kehrer L, Pinter P, et al. On the effective elastic properties based on mean-field homogenization of sheet molding compound composites. *Composites Part C: Open Access* 2021; 4(100089): 1–8.
3. Görthofer J, Meyer N, Pallicity TD, et al. Virtual process chain of sheet molding compound: Development, validation and perspectives. *Compos B Eng* 2019; 169: 133–147.
4. Lim LT, Britt IJ and Tung MA. Sorption and transport of water vapor in nylon 6,6 film. *J Appl Polym Sci* 1999; 71(2): 197–206.
5. Ehrenstein GW, Riedel G and Trawiel P. *Thermal analysis of plastics: Theory and practice*. München: Carl Hanser Verlag GmbH Co KG, 2012.
6. Vlasveld D, Groenewold J, Bersee H, et al. Moisture absorption in polyamide-6 silicate nanocomposites and its influence on the mechanical properties. *Polymer* 2005; 46(26): 12567–12576.
7. Brinson H and Brinson L. *Polymer engineering science and viscoelasticity: An introduction*. New York: Springer, 2015.
8. Ferry J. *Viscoelastic properties of polymers*. New York: John Wiley & Sons, 1980.
9. Tschoegl N. *The phenomenological theory of linear viscoelastic behavior*. Berlin: Springer, 1989.
10. Schapery RA. On the characterization of nonlinear viscoelastic materials. *Polym Eng Sci* 1969; 9(4): 295–310.
11. Serra-Aguila A, Puigoriol-Forcada JM, Reyes G, et al. Viscoelastic models revisited: characteristics and interconversion formulas for generalized Kelvin–Voigt and Maxwell models. *Acta Mech Sin* 2019; 35(6): 1191–1209.
12. Tschoegl N, Knauss WG and Emri I. Poisson's ratio in linear viscoelasticity – a critical review. *Mech Time-Depend Mat* 2002; 6(1): 3–51.
13. Kießling R and Ihlemann J. The dependence of the viscoelastic properties of polyamide 6 on temperature and moisture content: experiment and modeling. *Mater Today: Proc* 2020; 32: 83–87.
14. Koyanagi J, Hasegawa K, Ohtani A, et al. Formulation of non-linear viscoelastic-viscoplastic constitutive equation for polyamide 6 resin. *Heliyon* 2021; 7(2 e06335): 1–6.
15. Banks HT, Hu S and Kenz ZR. A brief review of elasticity and viscoelasticity for solids. *Adv Appl Math Mech* 2011; 3(1): 1–51.
16. Zink T, Kehrer L, Hirschberg V, et al. Nonlinear Schapery viscoelastic material model for thermoplastic polymers. *J Appl Polym Sci* 2022; 139(17): 1–7.
17. Aili A, Vandamme M, Torrenti JM, et al. Theoretical and practical differences between creep and relaxation poisson's ratios in linear viscoelasticity. *Mech Time-Depend Mat* 2015; 19(4): 537–555.
18. Kehrer L, Wicht D, Wood JT, et al. Dynamic mechanical analysis of pure and fiber-reinforced thermoset- and thermoplastic-based polymers and free volume-based viscoelastic modeling. *GAMM-Mitteilungen* 2018; 41(1): 1–16.

19. Dealy J and Plazek D. Time-temperature superposition - A users guide. *Rheology Bulletin* 2009; 78(2): 16–31.
20. Suarez-Afanador CA, Cornaggia R, Lahellec N, et al. Effective thermo-viscoelastic behavior of short fiber reinforced thermo-rheologically simple polymers: An application to high temperature fiber reinforced additive manufacturing. *Eur J Mech A Solids* 2022; 96: 104701.
21. Diani J, Gilormini P, Frédy C, et al. Predicting thermal shape memory of crosslinked polymer networks from linear viscoelasticity. *Int J Solids Struct* 2012; 49(5): 793–799.
22. Hu XL, Luo WB, Liu X, et al. Temperature and frequency dependent rheological behaviour of carbon black filled natural rubber. *Plast Rubber Compos* 2013; 42(10): 416–420.
23. Wortmann FJ and Schulz K. Investigations on the thermorheological simplicity of polypropylene fibres in the α-transition range. *Polymer* 1995; 36(8): 1611–1615.
24. Williams ML, Landel RF and Ferry JD. The temperature dependence of relaxation mechanisms in amorphous polymers and other glass-forming liquids. *J Am Chem Soc* 1955; 77(14): 3701–3707.
25. Alwis KGNC and Burgoyne CJ. Time-temperature superposition to determine the stress-rupture of aramid fibres. *Appl Compos Mater (Dordr)* 2006; 13(4): 249–264.
26. F Mano J and Viana J. Effects of the strain rate and temperature in stress–strain tests: Study of the glass transition of a polyamide-6. *Polym Test* 2001; 20(8): 937–943.
27. Serra-Aguila A, Puigoriol-Forcada JM, Reyes G, et al. Estimation of tensile modulus of a thermoplastic material from dynamic mechanical analysis: Application to polyamide 66. *Polymers* 2022; 14(6): 1210–1218.
28. Kristiawan M, Chaunier L, Della Valle G, et al. Linear viscoelastic properties of extruded amorphous potato starch as a function of temperature and moisture content. *Rheol Acta* 2016; 55(7): 597–611.
29. Shangguan Y, Chen F, Jia E, et al. New insight into time-temperature correlation for polymer relaxations ranging from secondary relaxation to terminal flow: Application of a universal and developed WLF equation. *Polymers* 2017; 9(11 567): 1–21.
30. Cole KS and Cole RH. Dispersion and absorption in dielectrics I. Alternating current characteristics. *J Chem Phys* 1941; 9(4): 341–351.
31. Guedes RM. A viscoelastic model for a biomedical ultra-high molecular weight polyethylene using the time–temperature superposition principle. *Polym Test* 2011; 30(3): 294–302.
32. Sodeifian G and Haghtalab A. Discrete relaxation spectrum and K-BKZ constitutive equation for PVC, NBR and their blends. *Appl Rheol* 2004; 14(4): 180–189.
33. van Gurp M and Palmen J. Time-temperature superposition for polymeric blends. *Rheology Bulletin* 1998; 67: 5–8.
34. Rouleau L, Deü JF, Legay A, et al. Application of Kramers–Kronig relations to time–temperature superposition for viscoelastic materials. *Mech Mater* 2013; 65: 66–75.
35. Capodagli J and Lakes R. Isothermal viscoelastic properties of PMMA and LDPE over 11 decades of frequency and time: a test of time–temperature superposition. *Rheol Acta* 2008; 47(7): 777–786.
36. Fabre V, Quandalle G, Billon N, et al. Time-temperature-water content equivalence on dynamic mechanical response of polyamide 6,6. *Polymer* 2018; 137: 22–29.
37. Kasapis S. Advanced topics in the application of the WLF/free volume theory to high sugar/biopolymer mixtures: A review. *Food Hydrocoll* 2001; 15(4–6): 631–641.

38. Zheng G, Kang Y and Sheng J. Influence of moisture content and time on the mechanical behavior of polymer material. *Sci China Ser E* 2004; 47(5): 595–607.
39. Ishisaka A and Kawagoe M. Examination of the time-water content superposition on the dynamic viscoelasticity of moistened polyamide 6 and epoxy. *J Appl Polym Sci* 2004; 93(2): 560–567.
40. Walter H, Dermitzaki E, Wunderle B, et al. Influence of moisture on humidity sensitive material parameters of polymers used in microelectronic applications. In 3rd Electronic System-Integration Technology Conference (ESTC). Piscataway, NJ: IEEE, pp. 1–5.
41. Ferry JD and Stratton RA. The free volume interpretation of the dependence of viscosities and viscoelastic relaxation times on concentration, pressure, and tensile strain. *Kolloid-Zeitschrift* 1960; 171(2): 107–111.
42. Popelar CF and Liechti KM. A distortion-modified free volume theory for nonlinear viscoelastic behavior. *Mech Time-Depend Mat* 2003; 7(2): 89–141.
43. Wenbo L, Ting-Qing Y and Qunli A. Time-temperature-stress equivalence and its application to nonlinear viscoelastic materials. *Acta Mech Solida Sin* 2001; 14(3): 195–199.
44. Chevali VS, Dean DR and Janowski GM. Flexural creep behavior of discontinuous thermoplastic composites: Non-linear viscoelastic modeling and time–temperature–stress superposition. *Compos Part A Appl Sci Manuf* 2009; 40(6–7): 870–877.
45. Ikeshima D, Matsuzaki A, Nagakura T, et al. Nonlinear creep deformation of polycarbonate at high stress level: Experimental investigation and finite element modeling. *J Mater Eng Perform* 2019; 28(3): 1612–1617.
46. Luo W, Wang C, Hu X, et al. Long-term creep assessment of viscoelastic polymer by time-temperature-stress superposition. *Acta Mech Solida Sin* 2012; 25(6): 571–578.
47. Hadid M, Guerira B, Bahri M, et al. The creep master curve construction for the polyamide 6 by the stepped isostress method. *Mat Res Innov* 2014; 18(6): S6-336–S6-339.
48. Monson L, Braunwarth M and Extrand CW. Moisture absorption by various polyamides and their associated dimensional changes. *J Appl Polym Sci* 2008; 107(1): 355–363.
49. Jia N, Fraenkel HA and Kagan VA. Effects of moisture conditioning methods on mechanical properties of injection molded nylon 6. *J Reinf Plast Compos* 2004; 23(7): 729–737.
50. Rösler J, Harders H and Bäker M. *Mechanical behaviour of engineering materials: metals, ceramics, polymers, and composites*. Berlin: Springer, 2007.
51. Kelley FN and Bueche F. Viscosity and glass temperature relations for polymer-diluent systems. *J Polym Sci (2020)* 1961; 50(154): 549–556.
52. Reimschuessel HK. Relationships on the effect of water on glass transition temperature and young's modulus of nylon 6. *J Polym Sci Polym Chem Ed* 1978; 16(6): 1229–1236.
53. Picard E, Gérard JF and Espuche E. Water transport properties of polyamide 6 based nanocomposites prepared by melt blending: On the importance of the clay dispersion state on the water transport properties at high water activity. *J Membr Sci* 2008; 313(1–2): 284–295.
54. Preda FM, Alegria A, Bocahut A, et al. Investigation of water diffusion mechanisms in relation to polymer relaxations in polyamides. *Macromolecules* 2015; 48(16): 5730–5741.
55. Lion A and Johlitz M. On the thermomechanics of solids surrounded by liquid media: balance equations, free energy and nonlinear diffusion. *Contin Mech Thermodyn* 2020; 32(2): 281–305.
56. Alfrey T, Gurnee E and Lloyd W. Diffusion in glassy polymers. In. *J Polym Sci C Polym Symp*. Wiley Online Library, 1966, 12, pp. 249–261.

57. Broudin M, Le Gac PY, Le Saux V, et al. Water diffusivity in PA66: Experimental characterization and modeling based on free volume theory. *Eur Polym J* 2015; 67: 326–334.
58. Fan X. Mechanics of moisture for polymers: fundamental concepts and model study. In EuroSimE 2008-International Conference on Thermal, Mechanical and Multi-Physics Simulation and Experiments in Microelectronics and Micro-Systems. IEEE, pp. 1–14.
59. Crank J. *The mathematics of diffusion*. New York: Oxford University Press, 1979.
60. Arhant M, Le Gac PY, Le Gall M, et al. Modelling the non Fickian water absorption in polyamide 6. *Polym Degrad Stab* 2016; 133: 404–412.
61. Venoor V, Park JH, Kazmer DO, et al. Understanding the effect of water in polyamides: A review. *Polym Rev* 2021; 61(3): 598–645.
62. Sharma P, Sambale A, Stommel M, et al. Moisture transport in PA6 and its influence on the mechanical properties. *Contin Mech Thermodyn* 2020; 32(2): 307–325.
63. Sharma P and Diebels S. A mixture theory for the moisture transport in polyamide. *Contin Mech Thermodyn* 2021; 33(4): 1891–1905.
64. Sambale A, Kurkowski M and Stommel M. Determination of moisture gradients in polyamide 6 using StepScan DSC. *Thermochim Acta* 2019; 672: 150–156.
65. Sambale AK, Maisl M, Herrmann HG, et al. Characterisation and modelling of moisture gradients in polyamide 6. *Polymers* 2021; 13(18): 3141.
66. Sambale AK, Stanko M, Emde J, et al. Characterisation and FE modelling of the sorption and swelling behaviour of polyamide 6 in water. *Polymers* 2021; 13(9): 1480.
67. Engelhard M and Lion A. Modelling the hydrothermomechanical properties of polymers close to glass transition. *Z Angew Math Mech* 2013; 93(2–3): 102–112.
68. ISO 62. Plastics – determination of water absorption (ISO 62:2008(E)), 2008.
69. ISO 291. Plastics – standard atmospheres for conditioning and testing (ISO 291:2008(E)), 2008.
70. ISO 1110. Plastics – polyamides – accelerated conditioning of test specimens (ISO 1110: 2019(E)), 2019.
71. Dijkstra DJ. Guidelines for rheological characterization of polyamide melts (IUPAC technical report). *Pure Appl Chem* 2009; 81(2): 339–349.
72. Menard K. *Dynamic mechanical analysis: A practical introduction*. Boca Raton: CRC Press, 2008.
73. Jia N and Kagan V. Mechanical performance of polyamides with influence of moisture and temperature–accurate evaluation and better understanding. *Plastics Failure Analysis and Prevention* 2001; 1: 95–104.
74. Domininghaus H. *Kunststoffe: Eigenschaften und Anwendungen*. Berlin: Springer, 2012.
75. Cho K. Geometric interpretation of time-temperature superposition. *Korea-Aust Rheol J* 2009; 21(1): 13–16.
76. Bae JE, Cho KS, Seo KH, et al. Application of geometric algorithm of time-temperature superposition to linear viscoelasticity of rubber compounds. *Korea-Aust Rheol J* 2011; 23(2): 81–87.
77. Maiti A. Second-order statistical bootstrap for the uncertainty quantification of time-temperature-superposition analysis. *Rheol Acta* 2019; 58(5): 261–271.
78. Gergesova M, Zupančič B, Saprunov I, et al. The closed form t-T-P shifting (CFS) algorithm. *J Rheol* 2011; 55(1): 1–16.
79. Gergesova M, Saprunov I and Emri I. Closed-form solution for horizontal and vertical shiftings of viscoelastic material functions in frequency domain. *Rheol Acta* 2016; 55(5): 351–364.

80. Oseli A, Aulova A, Gergesova M, et al. Time-temperature superposition in linear and nonlinear domain. *Mater Today: Proc* 2016; 3(4): 1118–1123.
81. Honerkamp J and Weese J. A note on estimating mastercurves. *Rheol Acta* 1993; 32(1): 57–64.
82. Sihn S and Tsai S. Automated shift for time-temperature superposition. In Proceedings of the 12th International Conference on Composite Materials. pp. 1–11.
83. Caracciolo R and Giovagnoni M. Frequency dependence of poisson's ratio using the method of reduced variables. *Mech Mater* 1996; 24(1): 75–85.
84. Hermida ÉB and Povolo F. Analytical-numerical procedure to determine if a set of experimental curves can be superimposed to form a master curve. *Polym J* 1994; 26(9): 981–992.
85. Naya S, Meneses A, Tarrío-Saavedra J, et al. New method for estimating shift factors in time–temperature superposition models. *J Therm Anal Calorim* 2013; 113(2): 453–460.
86. Honerkamp J and Weese J. Determination of the relaxation spectrum by a regularization method. *Macromolecules* 1989; 22(11): 4372–4377.
87. Ghobadi E, Sivanesapillai R, Musialak J, et al. Thermo-rheological characterization of polyetherurethane: Parameter optimization and validation. In B Marvalova and I Petrikova (eds.) *Constitutive models for rubbers IX*. Leiden: CRC Press/Balkema, 2015. pp. 157–163.
88. Jalocha D, Constantinescu A and Neviere R. Revisiting the identification of generalized maxwell models from experimental results. *Int J Solids Struct* 2015; 67-68: 169–181.
89. Bradshaw R and Brinson L. A sign control method for fitting and interconverting material functions for linearly viscoelastic solids. *Mech Time-Depend Mat* 1997; 1(1): 85–108.
90. Honerkamp J and Weese J. Tikhonovs regularization method for ill-posed problems. *Contin Mech Thermodyn* 1990; 2(1): 17–30.
91. Göhler J. Das dreidimensionale Stoffverhalten im großen Temperatur- und Zeitbereich am Beispiel eines in der automobilen Aufbau- und Verbindungstechnik verwendeten Epoxidharzklebstoffs. *Berichte aus der Materialwissenschaft*, Aachen: Shaker, 2011.
92. Zink T. Thermomechanische Modellierung von Polyamid 6. Bachelor Thesis, Institute of Engineering Mechanics, Chair for Continuum Mechanics, Karlsruhe Institute of Technology (KIT) 2021.
93. Hartmann S and Gilbert RR. Identifiability of material parameters in solid mechanics. *Arch Appl Mech* 2018; 88(1–2): 3–26.
94. Ehrenstein Studientexte Kunststofftechnik G. *Polymerwerkstoffe*. München: Hanser-Verlag, 1999.

Appendix

Cole-Cole plots for DAM samples

To check if application of TTS is valid, Cole-Cole plots are used.[31–33] Temperature-frequency sweeps with $\varepsilon_0 \leq 0.3\%$ show Cole-Cole plots with a smooth middle part (Figure 14). This indicates that TTS can be applied at the corresponding temperature levels. At the left end, data points are stacked. At the right end, the curve is not smooth. Thus, the corresponding temperature levels are neglected for the master curve. Figure 15 shows that TTS is invalid for the highest load.

Master curves for humidity-independent reference temperatures

In Figure 9, a moisture-dependent reference temperature is used. Alternatively, a constant reference temperature can be used, cf. Figure 16. Then, a shift caused by various moisture contents can be seen.

Maxwell parameters from parameter identification

In Table 8 and Table 9, the values of the parameter fits presented in Figures 11(e) and 13 are listed. The relaxation times were prescribed by a logarithmically equidistant distribution. The smallest (largest) relaxation time is defined by the inverse of the highest (lowest) frequency decade.

Sample thickness

In Table 10, the thickness of the respective sample used for the DMA tests is documented.

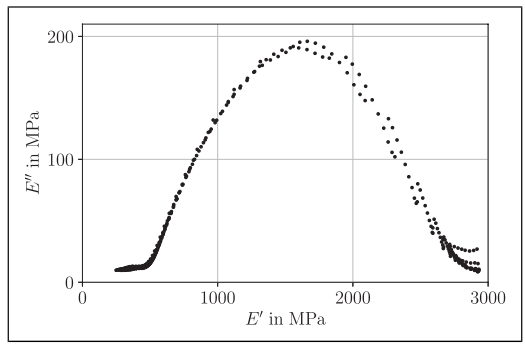

Figure 14. Cole-Cole plot indicates that TTS is valid: DAM, ε_0 = 0.1%.

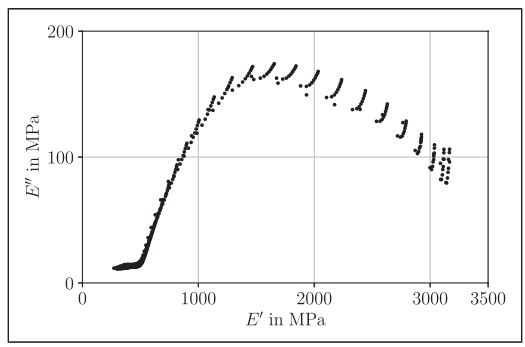

Figure 15. Cole-Cole plot shows that TTS is invalid: DAM, ε_0 = 0.5%.

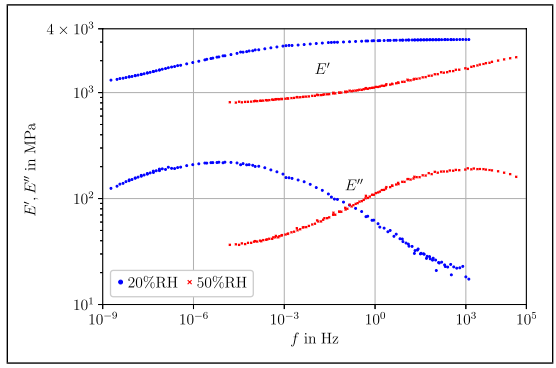

Figure 16. Master curves obtained from DMA testing with humidity control at a reference temperature of 30°C. A common master curve can be constructed by shifting the red curve to the right.

Table 8. DAM, $\varepsilon_0 = 0.1\%$, $a' = a'' = 0.5$.

GMM parameters for Figure 11(e)					
i	E_i in MPa	τ_i in s	i	E_i in MPa	τ_i in s
0	459.2				
1	22.41	1.0×10^{-12}	16	158.64	6.72×10^{-3}
2	6.29	4.52×10^{-12}	17	140.45	3.04×10^{-2}
3	16.97	2.04×10^{-11}	18	118.99	1.37×10^{-1}
4	14.1	9.24×10^{-11}	19	99.85	6.21×10^{-1}
5	20.76	4.18×10^{-10}	20	80.91	2.81
6	24.42	1.89×10^{-9}	21	63.24	1.27×10^{1}
7	31.83	8.53×10^{-9}	22	48.31	5.74×10^{1}
8	43.89	3.86×10^{-8}	23	36.14	2.59×10^{2}
9	55.77	1.74×10^{-7}	24	27.65	1.17×10^{3}
10	79.57	7.88×10^{-7}	25	21.15	5.3×10^{3}
11	102.59	3.56×10^{-6}	26	17.75	2.4×10^{4}
12	131.95	1.61×10^{-5}	27	15.33	1.08×10^{5}
13	157.2	7.28×10^{-5}	28	13.75	4.89×10^{5}
14	170.07	3.29×10^{-4}	29	13.92	2.21×10^{6}
15	170.95	1.49×10^{-3}	30	16.61	1.0×10^{7}

Table 9. DAM, ε_0 = 0.3%, $a' = a'' = 0.5$.

GMM parameters for Figure 13					
i	E_i in MPa	τ_i in s	i	E_i in MPa	τ_i in s
0	422.8				
1	87.53	1.0×10^{-15}	16	169.1	2.4×10^{-4}
2	71.48	5.74×10^{-15}	17	156.97	1.37×10^{-3}
3	82.1	3.29×10^{-14}	18	134.69	7.88×10^{-3}
4	88.36	1.89×10^{-13}	19	113.74	4.52×10^{-2}
5	91.56	1.08×10^{-12}	20	95.46	2.59×10^{-1}
6	95.7	6.21×10^{-12}	21	76.64	1.49
7	97.8	3.56×10^{-11}	22	60.24	8.53
8	102.15	2.04×10^{-10}	23	45.85	4.89×10^{1}
9	103.13	1.17×10^{-9}	24	34.47	2.81×10^{2}
10	112.57	6.72×10^{-9}	25	25.66	1.61×10^{3}
11	119.26	3.86×10^{-8}	26	20.62	9.24×10^{3}
12	131.55	2.21×10^{-7}	27	16.83	5.3×10^{4}
13	146.83	1.27×10^{-6}	28	15.04	3.04×10^{5}
14	162.89	7.28×10^{-6}	29	14.55	1.74×10^{6}
15	172.77	4.18×10^{-5}	30	17.01	1.0×10^{7}

Table 10. Sample thicknesses for the respective DMA tests.

Experiment type	Sample	Test	Thickness, mm
Relaxation from Figure 2	P12-41	20°C	2.06
	P12-40	40°C	2.06
	P12-48	60°C	2.07
	P12-5	80°C	2.06
	P3-18	80°C HC	2.08
Temp.-frequ. Sweep from Figures 3 and 4	P1-D-1	DAM	2.02
	P12-18	ATM-23/50	2.10
Humidity sweep from Figure 5	P1-56	20°C	2.11
	P1-55	40°C	2.15
	P10-13	60°C	2.16
	P10-20	80°C	2.19